

Reconstructing Non-standard Cosmologies with Dark Matter

Paola Arias,^a Nicolás Bernal,^b
Alan Herrera,^{b,c} Carlos Maldonado^a

^aDepartamento de Física, Universidad de Santiago de Chile,
Casilla 307, Santiago, Chile

^bCentro de Investigaciones, Universidad Antonio Nariño,
Carrera 3 Este # 47A-15, Bogotá, Colombia

^cDepartment of Physics and Astronomy, University of Rochester,
Rochester, NY 14627, USA.

E-mail: paola.arias.r@usach.cl, nicolas.bernal@uan.edu.co,
aherrer9@ur.rochester.edu, carlos.maldonados@usach.cl

Abstract. Once dark matter has been discovered and its particle physics properties have been determined, a crucial question rises concerning how it was produced in the early Universe. If its thermally averaged annihilation cross section is in the ballpark of $\text{few} \times 10^{-26} \text{ cm}^3/\text{s}$, the WIMP mechanism in the standard cosmological scenario (i.e. radiation dominated Universe) will be highly favored. If this is not the case one can either consider an alternative production mechanism, or a non-standard cosmology. Here we study the dark matter production in scenarios with a non-standard expansion history. Additionally, we reconstruct the possible non-standard cosmologies that could make the WIMP mechanism viable.

Contents

1	Introduction	1
2	Non-Standard Cosmologies	3
3	Reconstructing Cosmological Parameters	5
3.1	Classification	6
3.1.1	Case 1: $T_{\text{eq}} \ll T_{\text{fo}}$	6
3.1.2	Case 2: $T_c \ll T_{\text{fo}} \ll T_{\text{eq}}$	8
3.1.3	Case 3: $T_{\text{end}} \ll T_{\text{fo}} \ll T_c$	9
3.1.4	Case 4: $T_{\text{fo}} \ll T_{\text{end}}$	11
3.2	Varying the Particle Physics Parameters	11
3.3	Varying the Non-standard Cosmological Parameters	13
4	Conclusions	16

1 Introduction

There is compelling evidence for the existence of Dark Matter (DM), an unknown, non-baryonic matter component whose abundance in the Universe exceeds the amount of ordinary matter roughly by a factor of five [1]. In the previous decades a class of scenarios where dark and visible matter were once in thermal equilibrium with each other has received by far the biggest attention, both theoretically and experimentally. Most prominent in this class are extensions of the Standard Model of particle physics (SM) that feature Weakly Interacting Massive Particles (WIMPs) as DM [2–5].

Despite the fact that WIMP DM has been searched for decades, the studies have yielded no overwhelming evidence for what DM actually is. A crucial challenge to the WIMP DM paradigm is the lack of a confirmed experimental detection signal. The worldwide program for detecting WIMP DM using a multi-channel and multi-messenger approach has followed three main strategies: direct detection, indirect detection, and production at colliders.

However, the observed DM abundance may have been generated also out of equilibrium by a mechanism like the so-called freeze-in [6–12] (for a recent review see ref. [13]). Another simple way to evade the experimental constraints on DM is to consider non-standard cosmological histories, for example scenarios where the Universe was effectively matter-dominated at an early stage, due to a slow reheating period after inflation or to a massive metastable particle. There are no reasons to assume that the Universe was radiation-dominated prior to Big Bang Nucleosynthesis (BBN).¹

Examples of non-standard cosmologies are abundant in the literature. For instance, in typical string theory models there are many scalar moduli fields, the mass of which is typically set by the gravitino mass. If this is fairly low, motivated for example by the success of gauge unification in supersymmetric extensions of the SM, the moduli naturally dominate the energy density of the Universe at early times leading to an extended period of matter domination.

¹For studies on baryogenesis with a low reheating temperature or during an early matter-dominated phase, see refs. [14–18] and [19], respectively. Additionally, primordial gravitational wave production in scenarios with an early matter era have recently received particular attention [20–25].

The moduli eventually decay through Planck suppressed operators, and a radiation dominated Universe re-emerges before BBN. Additionally, in the kination scenario [26, 27] ϕ is a ‘fast-rolling’ field whose kinetic energy governs the expansion rate of the post-inflation Universe, with an equation of state $\omega = 1$. Due to the scaling of the energy density in radiation with the scale factor $\rho_R \propto a^{-4}$, which is slower than the scaling of the energy density in the ϕ field $\rho_\phi \propto a^{-6}$, the contribution from the radiation energy density in determining the expansion rate eventually becomes more important than that from the ϕ field. When the ϕ field redshifts away, the standard radiation dominated cosmology takes place. In general, production of DM in scenarios with a non-standard expansion phase has recently gained increasing interest, see e.g. refs. [28–53]. For earlier works, see also refs. [26, 54–64]. Additionally, a non-standard period might have lasted for a considerable amount of time, namely since the end of inflation down to the moment when BBN started [15, 65–68]. In these modified cosmologies, various properties of the WIMPs like their free-streaming velocity and the temperature at which the kinetic decoupling occurs have been investigated [69–72].

If DM is a WIMP that is a thermal relic of the early Universe, then its total thermally averaged self-annihilation cross section $\langle\sigma v\rangle$ is revealed by its present-day mass density. In standard cosmological scenarios, this result for a generic WIMP is usually stated as $\langle\sigma v\rangle_0 = \text{few} \times 10^{-26} \text{ cm}^3/\text{s} = \text{few} \times 10^{-9} \text{ GeV}^{-2}$, with a small logarithmic dependence of WIMP mass [73]. If $\langle\sigma v\rangle \gg \langle\sigma v\rangle_0$, DM is kept in chemical equilibrium with the thermal bath for longer, giving rise to a DM underabundance that can be understood for example in the context of multicomponent DM. On the contrary, if $\langle\sigma v\rangle \ll \langle\sigma v\rangle_0$, DM decouples earlier and generates an overabundance that overcloses the Universe. In non-standard cosmologies, however, the generic value for $\langle\sigma v\rangle_0$ does not hold anymore, strongly depending on the details of the cosmology.

Once DM is discovered and its particle physics properties have been reconstructed (i.e. mass and couplings with the SM), a major question rises concerning the DM production mechanism.² If the inferred value of $\langle\sigma v\rangle$ is in the ballpark of $\langle\sigma v\rangle_0$, the simpler freeze-out mechanism with a standard cosmology will be strongly favored. However, if that turns out not to be the case, one can either look for different DM production mechanisms or for alternative cosmological scenarios. The latter option will be pursued in this study.

In this paper we consider production of WIMP DM in scenarios where for some period at early times (for temperatures around the DM mass) the expansion of the Universe was governed by a component ϕ with an effective equation of state $\omega = p_\phi/\rho_\phi$, where p_ϕ is the pressure and ρ_ϕ the energy density of ϕ . Using a particle physics model independent approach, for a given DM mass m and a thermally averaged DM annihilation cross section $\langle\sigma v\rangle$, we study the capabilities for reconstructing the parameters characterizing the non-standard cosmology. The paper is organized as follows: In section 2 we introduce the cosmological setup. In section 3 we present the reconstruction capabilities of the cosmological parameters. Finally, we conclude in section 4.

²It is necessary to make use of the complementarity between different experiments and different detection techniques [74–90] in order to ameliorate determination of the particle physics parameters and disentangle possible degeneracies. Furthermore, one has to take into account astrophysical uncertainties [91–106] when interpreting the results of the DM searches.

2 Non-Standard Cosmologies

We assume that for some period of the early Universe, the total energy density was dominated by a component ρ_ϕ with an equation of state parameter ω , where $\omega \equiv p_\phi/\rho_\phi$, with p_ϕ the pressure of the dominant component. Additionally, this component decays with a total rate Γ_ϕ .

In the early Universe the evolution of the ϕ energy density ρ_ϕ , the SM entropy density s , as well as the DM number density n are governed by the system of coupled Boltzmann equations [15, 40]

$$\frac{d\rho_\phi}{dt} + 3(1 + \omega) H \rho_\phi = -\Gamma_\phi \rho_\phi, \quad (2.1)$$

$$\frac{ds}{dt} + 3 H s = +\frac{\Gamma_\phi \rho_\phi}{T} \left(1 - b \frac{E}{m_\phi}\right) + 2 \frac{E}{T} \langle \sigma v \rangle (n^2 - n_{\text{eq}}^2), \quad (2.2)$$

$$\frac{dn}{dt} + 3 H n = +\frac{b}{m_\phi} \Gamma_\phi \rho_\phi - \langle \sigma v \rangle (n^2 - n_{\text{eq}}^2), \quad (2.3)$$

where $\langle \sigma v \rangle$ is the total DM annihilation cross-section into SM particles and $E^2 \simeq m^2 + 3T^2$ is the averaged energy per DM particle. In general ϕ decays into both SM radiation and DM particles [107], with a proportion controlled by the parameter b . In fact, b is twice the branching ratio of ϕ decaying into a couple of DM particles³ and m_ϕ corresponds to the mass of the state ϕ . Additionally, $1 - b E/m_\phi$ is the fraction of ρ_ϕ that goes into radiation. The second term in the RHS of eq. (2.2) corresponding to the entropy injection due to DM annihilations is subdominant and thus is ignored.

Additionally, the two terms in the RHS of eq. (2.3) represent the non-thermal production via the decay of ϕ , and the usual thermal WIMP production, respectively. However, here we focus in the case where DM is thermally produced, which implies that the branching ratio of ϕ into DM particles is subdominant, and therefore we disregard it, i.e. $b = 0$.⁴

Under the assumption that the SM plasma maintains internal equilibrium at all times in the early Universe, its temperature dependence can be obtained from its energy density

$$\rho_R(T) = \frac{\pi^2}{30} g_\star(T) T^4. \quad (2.4)$$

Equation (2.2) plays an important role in tracking the evolution of the photon's temperature T , via the SM entropy density s ,

$$s(T) = \frac{\rho_R + p_R}{T} = \frac{2\pi^2}{45} g_{\star S}(T) T^3, \quad (2.5)$$

where $g_\star(T)$ and $g_{\star S}(T)$ correspond to the effective number of relativistic degrees of freedom for SM energy and entropy densities, respectively [108]. The evolution of the SM temperature follows from Eq. (2.2):

$$\frac{dT}{da} = \left(1 + \frac{T}{3g_{\star S}} \frac{dg_{\star S}}{dT}\right)^{-1} \left[-\frac{T}{a} + \frac{\Gamma_\phi \rho_\phi}{3H s a} \left(1 - \frac{E b}{m_\phi}\right) + \frac{2E \langle \sigma v \rangle}{3H s a} (n^2 - n_{\text{eq}}^2) \right]. \quad (2.6)$$

³We assume here that the main decay channel of ϕ into DM particles is into two of them.

⁴Let us note that the decay into DM particles can be disregarded as long as $b < 10^{-4} m/(100 \text{ GeV})$ [40].

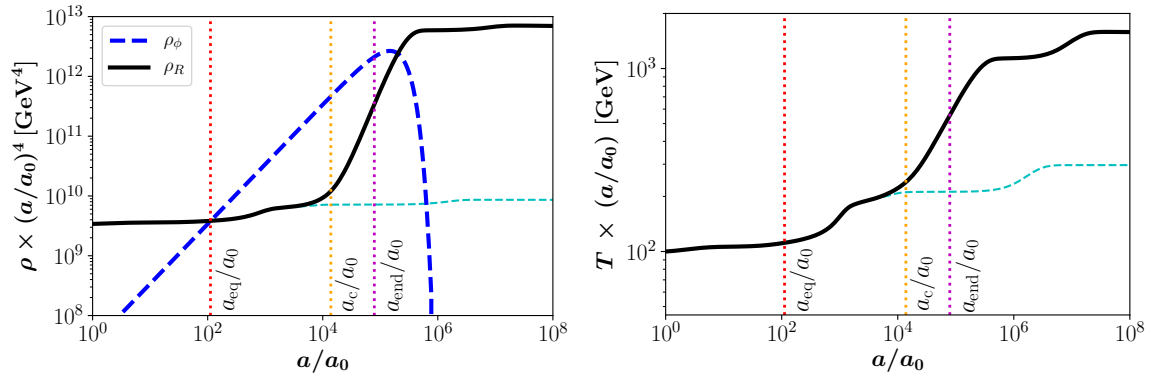


Figure 1. Evolution of the energy densities for radiation and the ϕ field (left panel), and evolution of the photon temperature T (right panel) as a function of the scale factor a , for $\omega = 0$, $T_{\text{end}} = 7 \times 10^{-3}$ GeV and $\frac{\rho_\phi}{\rho_R} \Big|_{T=100 \text{ GeV}} = 10^{-2}$. The cyan dashed lines represent the standard cosmological scenario without the ϕ field. Here we assume that $a_0 = a(T = 100 \text{ GeV})$. The scale factors $a = a_{\text{eq}}$, a_c and a_{end} are overlaid.

The Hubble expansion rate H is defined by

$$H^2 = \frac{\rho_\phi + \rho_R + \rho_\chi}{3 M_P^2}, \quad (2.7)$$

where M_P is the reduced Planck mass.

For having a successful BBN, the temperature at the end of the ρ_ϕ dominated phase has to be $T_{\text{end}} \gtrsim 4 \text{ MeV}$ [109–112], where T_{end} is given by the total decay width Γ_ϕ as

$$T_{\text{end}}^4 \equiv \frac{90}{\pi^2 g_*(T_{\text{end}})} M_P^2 \Gamma_\phi^2. \quad (2.8)$$

Let us note that for $\omega > 1/3$, ρ_ϕ gets diluted faster than radiation, and if $\rho_\phi \ll \rho_R$ at $T = T_{\text{BBN}}$, Γ_ϕ could be effectively taken to be zero.

As an example, fig. 1 shows the solution of the Boltzmann equations (2.1) and (2.2), for $\omega = 0$, $T_{\text{end}} = 7 \times 10^{-3}$ GeV and $\frac{\rho_\phi}{\rho_R} \Big|_{T=100 \text{ GeV}} = 10^{-2}$.⁵ The left panel depicts the evolution of the radiation and ϕ energy densities as a function of the scale factor a , taking $a_0 = a(T = 100 \text{ GeV})$. a_{eq} corresponds to the scale factor at which ρ_ϕ starts to dominate over ρ_R , a_c to the scale factor where effectively ρ_ϕ starts to dominate the evolution of ρ_R , and a_{end} is a proxy of the scale factor where ϕ decays completely. Additionally $T_{\text{eq}} \equiv T(a = a_{\text{eq}})$, $T_c \equiv T(a = a_c)$ and $T_{\text{end}} \equiv T(a = a_{\text{end}})$. T_{end} is properly defined in eq. (2.8). The photon temperature can be extracted from the radiation energy density using eq. (2.4) and it is depicted as a function of the scale factor in the right panel of fig. 1. The bumps at $a/a_0 \sim 10^3$ and $\sim 10^7$, corresponding to temperatures $T \sim 10^{-1}$ GeV and $\sim 10^{-3}$ GeV, are due to the QCD phase transition and the annihilation of electron-positron pairs, respectively. For completeness, we also show in the figure with cyan dashed lines the evolution of the SM energy density and the temperature in the case without the ϕ field. In the case with constant

⁵Let us emphasize that all the figures in this work were produced using the full numerical expressions.

relativistic degrees of freedom one has that $\rho_\phi(a) \propto a^{-3(1+\omega)}$ until it decays, and

$$\rho_R(a) \propto \begin{cases} a^{-4} & \text{for } a \ll a_c, \\ a^{-\frac{3}{2}(1+\omega)} & \text{for } a_c \ll a \ll a_{\text{end}}, \\ a^{-4} & \text{for } a_{\text{end}} \ll a, \end{cases} \quad (2.9)$$

which implies that

$$T(a) \propto \begin{cases} a^{-1} & \text{for } a \ll a_c, \\ a^{-\frac{3}{8}(1+\omega)} & \text{for } a_c \ll a \ll a_{\text{end}}, \\ a^{-1} & \text{for } a_{\text{end}} \ll a. \end{cases} \quad (2.10)$$

3 Reconstructing Cosmological Parameters

In order to have a successful WIMP mechanism, a thermally averaged annihilation cross section $\langle\sigma v\rangle \sim \text{few} \times 10^{-26} \text{ cm}^3/\text{s}$ is typically needed [73]. If a DM measurement points towards a significantly different value, the simplest WIMP scenario could still be the responsible for the DM genesis, but with a non-standard cosmological evolution.

Here, we assume that both the DM mass m and its thermally averaged annihilation cross section $\langle\sigma v\rangle$ are known after a discovery, and we try to reconstruct the non-standard cosmological parameters that make the DM genesis compatible with the WIMP paradigm. In this study we consider scenarios where for some period at early times the expansion of the Universe was governed by a fluid component with an effective equation of state ω . Particular cases correspond to $\omega = -1$ (quintessence), 0 (dust), $1/3$ (radiation) and 1 (kination). However, we will mainly focus on a phase of matter domination assuming $\omega = 0$.

The non-standard cosmologies considered here can be fully parametrized with three free parameters:

$$T_{\text{end}}, \quad \kappa \equiv \left. \frac{\rho_\phi}{\rho_R} \right|_{T=m} \quad \text{and} \quad \omega. \quad (3.1)$$

Figure 2 depicts in blue the parameter space compatible with the observed DM abundance via the WIMP mechanism with non-standard cosmologies, in the plane $[T_{\text{end}}, \kappa]$, assuming $\omega = 0$. For the particle physics benchmark we have chosen $m = 100 \text{ GeV}$ and $\langle\sigma v\rangle = 10^{-11} \text{ GeV}^{-2}$. The left part of the plot colored in gray and corresponding to $T_{\text{end}} < 4 \text{ MeV}$ is in tension with BBN. Additionally, in the lower right corner ρ_ϕ is always subdominant with respect to radiation, and hence corresponds to the usual case, radiation dominated.⁶ The figure also shows the lines corresponding to $T_{\text{fo}} = T_{\text{eq}}$, $T_{\text{fo}} = T_c$ and $T_{\text{fo}} = T_{\text{end}}$. These lines differentiate four phenomenologically distinct regimes characterized by the temperature T_{fo} when the DM freeze-out happens, with respect to T_{eq} , T_c and T_{end} . These cases are described in detail in the next subsections, where analytic estimations of the different regimes are performed.⁷

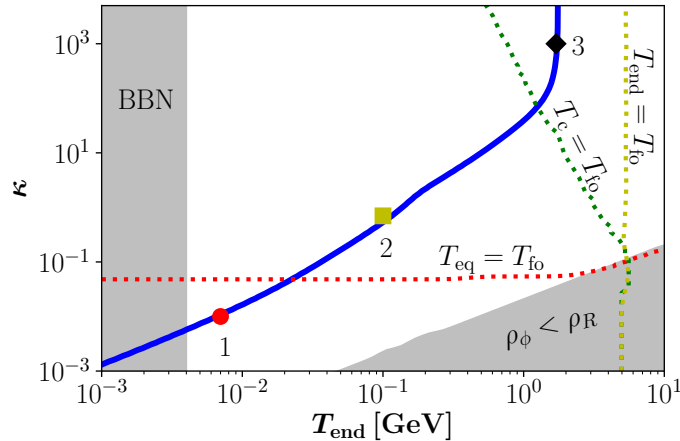


Figure 2. Parameter space generating the observed DM abundance via the WIMP mechanism with non-standard cosmologies, assuming $\omega = 0$. For the particle physics benchmark we have taken $m = 100$ GeV and $\langle\sigma v\rangle = 10^{-11}$ GeV $^{-2}$. The gray bands correspond to $T_{\text{end}} < T_{\text{BBN}}$ and $\rho_\phi < \rho_R$. Benchmarks 1, 2 and 3 are the parameters used in figs. 3 and 7. The lines corresponding to $T_{\text{fo}} = T_{\text{eq}}$, $T_{\text{fo}} = T_c$ and $T_{\text{fo}} = T_{\text{end}}$ are overlaid.

3.1 Classification

3.1.1 Case 1: $T_{\text{eq}} \ll T_{\text{fo}}$

The first case, characterized by $T_{\text{eq}} \ll T_{\text{fo}}$ is by far the most studied in the literature. It corresponds to the scenario where the DM freeze-out happens during radiation domination, and much earlier than the time when ϕ decays. The upper left panel of fig. 3 shows the evolution of the DM yield $Y \equiv n/s$ as a function of $x \equiv m/T$, for the benchmark point $m = 100$ GeV, $\langle\sigma v\rangle = 10^{-11}$ GeV $^{-2}$, $T_{\text{end}} = 7 \times 10^{-3}$ GeV, $\kappa = 10^{-2}$ and $\omega = 0$ (point 1 in fig. 2). The green horizontal band corresponds to the DM relic abundance, as measured by Planck [1]. Here the freeze-out happens as in the standard radiation dominated case, and it is succeeded by a dilution due to the entropy injection produced by the late decay of ϕ . Much before the decay of ϕ , the SM entropy is conserved and therefore the Boltzmann equation (2.3) can be rewritten as

$$\frac{dY}{dx} = -\frac{\langle\sigma v\rangle s}{H x} (Y^2 - Y_{\text{eq}}^2), \quad (3.2)$$

where $Y_{\text{eq}} \equiv n_{\text{eq}}/s$. Taking into account that $H \simeq \sqrt{\frac{\rho_R}{3M_P^2}} = \pi\sqrt{\frac{g_*}{90}} \frac{m^2}{M_P x^2}$, eq. (3.2) admits the standard approximate solution

$$Y_0 = \frac{15}{2\pi\sqrt{10} g_*} \frac{x_{\text{fo}}}{m M_P \langle\sigma v\rangle}, \quad (3.3)$$

where Y_0 corresponds to the DM yield long after the freeze-out, but before the decay of ϕ .

⁶That region can be understood in the sudden decay approximation, where the equality $\rho_R(a_{\text{end}}) = \rho_\phi(a_{\text{end}})$ takes place, implying that $\kappa = \frac{g_*(T_{\text{end}})}{g_*(m)} \left[\frac{T_{\text{end}}}{m}\right]^{1-3\omega}$.

⁷For the analytical estimations the variation of the number of relativistic degrees of freedom g_* and g_{*S} is ignored. Additionally, we will take $g_{*S} = g_*$, which is a good approximation for $T > 1$ MeV.

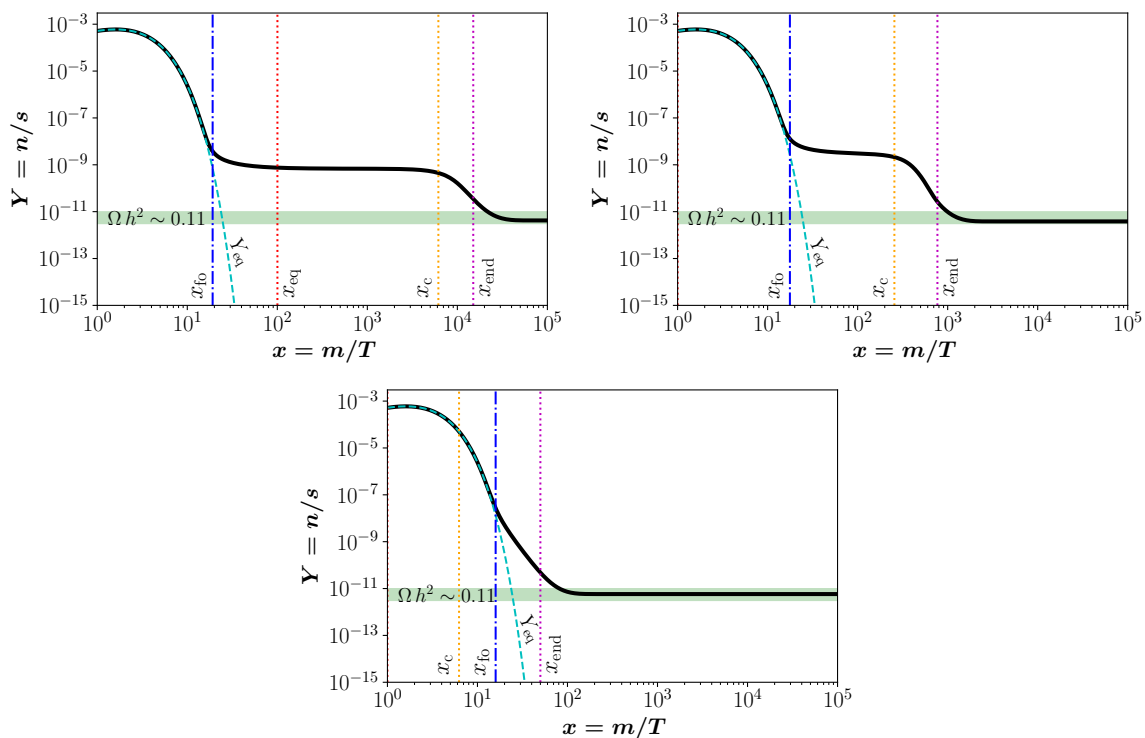


Figure 3. Evolution of the DM yield (thick black lines) as a function of the inverse of the temperature using $m = 100$ GeV and $\langle\sigma v\rangle = 10^{-11}$ GeV $^{-2}$, for the benchmark points shown in fig. 2. Upper left panel: $T_{\text{end}} = 7 \times 10^{-3}$ GeV and $\kappa = 10^{-2}$. Upper right panel: $T_{\text{end}} = 10^{-1}$ GeV and $\kappa = 1$. Lower panel: $T_{\text{end}} = 2$ GeV and $\kappa = 10^3$. Y_{eq} is also shown in dashed lines. x_{fo} , x_{eq} , x_c and x_{end} are also overlaid. The green horizontal bands correspond to the DM relic abundance, as measured by Planck.

Additionally, $x_{\text{fo}} \equiv m/T_{\text{fo}}$ is defined by $n_{\text{eq}}\langle\sigma v\rangle/H|_{x=x_{\text{fo}}} = 1$ and given by

$$x_{\text{fo}} = \ln \left[\frac{3}{2} \sqrt{\frac{5}{\pi^5 g_\star}} g m M_P \langle\sigma v\rangle \sqrt{x_{\text{fo}}} \right], \quad (3.4)$$

where g is the number of degrees of freedom for DM. In this first scenario, x_{fo} is independent on the cosmological parameters T_{end} , κ and ω , because the freeze-out happens in the standard cosmological scenario. At this point let us emphasize that the obtained DM abundance is much larger than the observed one (as we are assuming that $\langle\sigma v\rangle \ll \langle\sigma v\rangle_0$), and therefore has to be reduced.

The decay of ϕ dilutes the DM by injecting entropy to the SM bath. The dilution factor $D \equiv s(T_2)/s(T_1) = (T_2/T_1)^3$ is defined as the ratio of the SM entropies after and before the decay, and can be estimated as follows. In the sudden decay approximation of ϕ , the conservation of the energy density implies

$$\rho_R(T_1) + \rho_\phi(T_1) = \rho_R(T_2), \quad (3.5)$$

where T_1 and T_2 are the temperatures just before and just after ϕ decays, respectively. Taking

into account that the scaling of ρ_ϕ and that $\rho_\phi(m) = \kappa \rho_R(m)$, one gets that

$$D = \left(\frac{T_2}{T_1}\right)^3 \simeq \left[\kappa \left(\frac{m}{T_2}\right)^{1-3\omega} \right]^{\frac{1}{1+\omega}} \quad \text{for } \omega \neq -1, \quad (3.6)$$

$$D = \left(\frac{T_2}{T_1}\right)^3 = \left[1 - \kappa \left(\frac{m}{T_2}\right)^4 \right]^{-\frac{3}{4}} \quad \text{for } \omega = -1. \quad (3.7)$$

It can be checked that the choice $T_2 = T_{\text{end}}$ fits well the full numerical solution.

The final DM abundance given by the ratio of eqs. (3.3) and (3.6) or (3.7) has to match the observations by the Planck collaboration [1]

$$Y_{\text{obs}} = \frac{Y_0}{D} \simeq \frac{15}{2\pi\sqrt{10}g_\star} \frac{x_{\text{fo}}}{m M_P \langle\sigma v\rangle} \left[\frac{1}{\kappa} \left(\frac{T_{\text{end}}}{m}\right)^{1-3\omega} \right]^{\frac{1}{1+\omega}} \quad \text{for } \omega \neq -1, \quad (3.8)$$

$$Y_{\text{obs}} = \frac{Y_0}{D} = \frac{15}{2\pi\sqrt{10}g_\star} \frac{x_{\text{fo}}}{m M_P \langle\sigma v\rangle} \left[1 - \kappa \left(\frac{m}{T_{\text{end}}}\right)^4 \right]^{\frac{3}{4}} \quad \text{for } \omega = -1, \quad (3.9)$$

where $Y_{\text{obs}} \times m = \frac{\rho_c \Omega_{\text{DM}} h^2}{s_0 h^2} \simeq 4 \times 10^{-10}$ GeV, ρ_c is the critical energy density of the Universe, and s_0 and Ω_{DM} are the entropy density and the DM relic abundance nowadays, respectively. Previous equations implies that in scenario 1, in order to reproduce the observed DM abundance $\kappa \propto T_{\text{end}}^{1-3\omega}$. In the case where $\omega = 0$, $\kappa \propto T_{\text{end}}$ as observed in fig. 2.

3.1.2 Case 2: $T_c \ll T_{\text{fo}} \ll T_{\text{eq}}$

This case corresponds to the scenario where $T_c \ll T_{\text{fo}} \ll T_{\text{eq}}$. In this regime the Hubble expansion rate is driven by ρ_ϕ . However, ϕ is not yet efficiently decaying into SM radiation, so that T is still inversely proportional to the scale factor. The upper right panel of fig. 3 shows the evolution of the DM yield, for the benchmark point $m = 100$ GeV, $\langle\sigma v\rangle = 10^{-11}$ GeV $^{-2}$, $T_{\text{end}} = 10^{-1}$ GeV, $\kappa = 1$ and $\omega = 0$ (point 2 in fig. 2). Compared to the previous case, the main difference here is the expansion of the Universe. In fact, now

$$H \simeq \sqrt{\frac{\rho_\phi}{3M_P^2}} = \frac{\pi}{3} \sqrt{\frac{g_\star}{10}} \frac{m^2}{M_P} \sqrt{\frac{\kappa}{x^{3(1+\omega)}}}, \quad (3.10)$$

and therefore eq. (3.2) admits the approximate solutions

$$Y_0 = \frac{45}{4\pi} \frac{1-\omega}{m M_P \langle\sigma v\rangle} \sqrt{\frac{\kappa}{10g_\star}} x_{\text{fo}}^{\frac{3}{2}(1-\omega)} \quad \text{for } \omega \neq 1, \quad (3.11)$$

$$Y_0 = \frac{15}{2\pi} \frac{1}{m M_P \langle\sigma v\rangle} \sqrt{\frac{\kappa}{10g_\star}} \left[\ln \frac{x_{\text{end}}}{x_{\text{fo}}} \right]^{-1} \quad \text{for } \omega = 1. \quad (3.12)$$

The DM freeze-out happens at

$$x_{\text{fo}} = \ln \left[\frac{3}{2} \sqrt{\frac{5}{\pi^5 g_\star}} g \frac{m M_P \langle\sigma v\rangle}{\sqrt{\kappa}} x_{\text{fo}}^{\frac{3}{2}\omega} \right], \quad (3.13)$$

which depends only on κ . Figure 4 shows contour lines for $x_{\text{fo}} = 14$ (blue), 16 (black) and 18 (magenta) in the $[T_{\text{end}}, \kappa]$ plane, assuming $\omega = 0$ and numerically solving the full Boltzmann

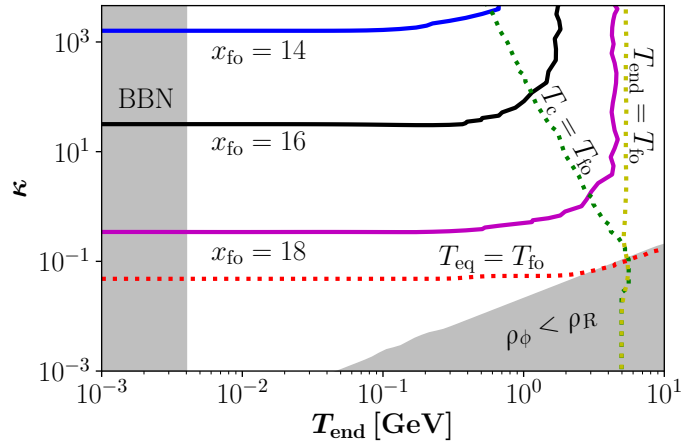


Figure 4. Contour lines for the inverse of the temperature at which the DM freeze-out occurs: $x_{\text{fo}} = 14$ (blue line), 16 (black line) and 18 (magenta line). We assumed $\omega = 0$, $m = 100$ GeV and $\langle\sigma v\rangle = 10^{-11}$ GeV $^{-2}$. The colored bands correspond to $T_{\text{end}} < T_{\text{BBN}}$ and $\rho_\phi < \rho_R$. The lines corresponding to $T_{\text{fo}} = T_{\text{eq}}$, $T_{\text{fo}} = T_c$ and $T_{\text{fo}} = T_{\text{end}}$ are overlaid.

equations. In the same way as in fig. 2, here we choose $m = 100$ GeV and $\langle\sigma v\rangle = 10^{-11}$ GeV $^{-2}$. The left part of the plot in gray, corresponding to $T_{\text{end}} < 4$ MeV, is in tension with BBN. Additionally, in the lower right corner ρ_ϕ is always subdominant with respect to radiation, and hence corresponds to the usual case, radiation dominated. The figure also shows the lines corresponding to $T_{\text{fo}} = T_{\text{eq}}$, $T_{\text{fo}} = T_c$ and $T_{\text{fo}} = T_{\text{end}}$. The κ dependence on eq. (3.13), for $T_c \ll T_{\text{fo}} \ll T_{\text{eq}}$, is shown in fig. 4 as horizontal lines.

The final DM abundance given by the ratio of eqs. (3.11), (3.12), (3.6) and (3.7) is given by

$$Y_{\text{obs}} = \frac{Y_0}{D} = \frac{45}{4\pi\sqrt{10g_\star}} \frac{\sqrt{\kappa}}{m M_P \langle\sigma v\rangle} x_{\text{fo}}^3 \left[1 - \kappa \left(\frac{m}{T_{\text{end}}} \right)^4 \right]^{\frac{3}{4}} \quad \text{for } \omega = -1, \quad (3.14)$$

$$Y_{\text{obs}} = \frac{Y_0}{D} \simeq \frac{45(1-\omega)}{4\pi\sqrt{10g_\star}} \frac{\sqrt{\kappa}}{m M_P \langle\sigma v\rangle} x_{\text{fo}}^{\frac{3}{2}(1-\omega)} \left[\frac{1}{\kappa} \left(\frac{T_{\text{end}}}{m} \right)^{1-3\omega} \right]^{\frac{1}{1+\omega}} \quad \text{for } |\omega| \neq 1, \quad (3.15)$$

$$Y_{\text{obs}} = \frac{Y_0}{D} \simeq \frac{15}{2\pi} \sqrt{\frac{1}{10g_\star}} \frac{1}{T_{\text{end}} M_P \langle\sigma v\rangle} \left[\ln \frac{T_{\text{fo}}}{T_{\text{end}}} \right]^{-1} \quad \text{for } \omega = 1. \quad (3.16)$$

Previous equations imply that in scenario 2, in order to reproduce the observed DM abundance $\kappa \propto T_{\text{end}}^{2\frac{1-3\omega}{1-\omega}}$. In the case of $\omega = 0$, $\kappa \propto T_{\text{end}}^2$ as observed in fig. 2, for $T_c \ll T_{\text{fo}} \ll T_{\text{eq}}$.

3.1.3 Case 3: $T_{\text{end}} \ll T_{\text{fo}} \ll T_c$

This case corresponds to the scenario where $T_{\text{end}} \ll T_{\text{fo}} \ll T_c$.⁸ In this regime ρ_ϕ controls both the Hubble expansion rate and the evolution of ρ_R . The lower panel of fig. 3 shows the evolution of the DM yield, for the benchmark point $m = 100$ GeV, $\langle\sigma v\rangle = 10^{-11}$ GeV $^{-2}$,

⁸It is interesting to note that this case is only possible for $\omega \neq -1$; in fact if $\omega = -1$, between a_c and a_{end} the temperature is independent of the scale factor (see eq. (2.10)) and therefore $T_c = T_{\text{end}}$.

$T_{\text{end}} = 2 \text{ GeV}$, $\kappa = 10^3$ and $\omega = 0$ (point 3 in fig. 2). As in this case the freeze-out occurs when the ϕ is decaying and the SM entropy is not conserved, one can not use anymore the Boltzmann equation (3.2). Instead, eq. (2.3) can be rewritten as

$$\frac{dN}{da} = -\frac{\langle\sigma v\rangle}{H a^4} (N^2 - N_{\text{eq}}^2), \quad (3.17)$$

where $N \equiv n \times a^3$ and similarly $N_{\text{eq}} \equiv n_{\text{eq}} \times a^3$. Taking into account that

$$H(a) \simeq \sqrt{\frac{\rho_\phi(a)}{3M_P^2}} = \sqrt{\frac{\rho_\phi(a_0)}{3M_P^2}} \left(\frac{a_0}{a}\right)^{\frac{3}{2}(1+\omega)} = \frac{\pi}{3} \sqrt{\kappa \frac{g_\star}{10}} \frac{m^2}{M_P} \left(\frac{a_0}{a}\right)^{\frac{3}{2}(1+\omega)}, \quad (3.18)$$

and choosing the scale factor such that $a_0 \equiv a(T = m) = 1$, eq. (3.17) admits the approximate solution

$$N_0 = \frac{(1-\omega)\pi}{2} \sqrt{\kappa \frac{g_\star}{10}} \frac{m^2}{M_P \langle\sigma v\rangle} \left(\frac{a_{\text{fo}}}{a_0}\right)^{\frac{3}{2}(1-\omega)} \quad \text{for } \omega \neq 1, \quad (3.19)$$

$$N_0 = \frac{\pi}{3} \sqrt{\kappa \frac{g_\star}{10}} \frac{m^2}{M_P \langle\sigma v\rangle} \left(\ln \frac{a_{\text{end}}}{a_{\text{fo}}}\right)^{-1} \quad \text{for } \omega = 1, \quad (3.20)$$

where N_0 corresponds to the value of N well after the DM freeze-out.

Within the sudden decay approximation and using eq. (2.10), the value of the critical temperature T_c and the scale factors at $T = T_{\text{fo}}$ and $T = T_{\text{end}}$ can be estimated as

$$T_c = (\kappa m^{1-3\omega} T_{\text{end}}^4)^{\frac{1}{5-3\omega}}, \quad (3.21)$$

$$a_{\text{fo}} = a_0 m \left(\frac{T_c^{5-3\omega}}{T_{\text{fo}}^8}\right)^{\frac{1}{3(1+\omega)}} = a_0 \left[\kappa \left(\frac{m T_{\text{end}}}{T_{\text{fo}}^2}\right)^4\right]^{\frac{1}{3(1+\omega)}}, \quad (3.22)$$

$$a_{\text{end}} = a_0 m \left(\frac{T_c^{5-3\omega}}{T_{\text{end}}^8}\right)^{\frac{1}{3(1+\omega)}} = a_0 \left[\kappa \left(\frac{m}{T_{\text{end}}}\right)^4\right]^{\frac{1}{3(1+\omega)}}. \quad (3.23)$$

The final DM yield Y_0 is related to N_0 via the factor $s \times a^3$, which after the decay of ϕ can be written as

$$s a^3 = \frac{2\pi^2}{45} g_\star (T_{\text{end}} a_{\text{end}})^3 = \frac{2\pi^2}{45} g_\star \left[\kappa \frac{m^4}{T_{\text{end}}^{1-3\omega}}\right]^{\frac{1}{1+\omega}}, \quad (3.24)$$

implying that

$$Y_{\text{obs}} = \frac{N_0}{s a^3} = \frac{45(1-\omega)}{4\pi} \sqrt{\frac{1}{10g_\star}} \frac{1}{M_P \langle\sigma v\rangle} \left[T_{\text{fo}}^{4(\omega-1)} T_{\text{end}}^{3-5\omega}\right]^{\frac{1}{1+\omega}} \quad \text{for } \omega \neq 1, \quad (3.25)$$

$$Y_{\text{obs}} = \frac{N_0}{s a^3} = \frac{45}{8\pi} \sqrt{\frac{1}{10g_\star}} \frac{1}{T_{\text{end}} M_P \langle\sigma v\rangle} \left(\ln \frac{T_{\text{fo}}}{T_{\text{end}}}\right)^{-1} \quad \text{for } \omega = 1, \quad (3.26)$$

which is independent of κ , as expected from fig. 2.

In order to estimate the temperature at which the DM freeze-out happens, let us first examine how ρ_ϕ scales. The evolution of ρ_ϕ has to be divided in two regimes (after and before $a = a_c$), because of the two different dependences on T :

$$\rho_\phi(a) = \rho_\phi(a_0) \left(\frac{a_0}{a}\right)^{3(1+\omega)} = \rho_\phi(a_0) \left(\frac{a_0 a_c}{a_c a}\right)^{3(1+\omega)}. \quad (3.27)$$

Using eqs. (2.10) and (3.21), eq. (3.27) can be rewritten as

$$\rho_\phi(T) = \rho_\phi(m) \left(\frac{T_c}{m}\right)^{3(1+\omega)} \left(\frac{T}{T_c}\right)^8 = \frac{\pi^2 g_\star}{30} \kappa m^{1-3\omega} \frac{T^8}{T_c^{5-3\omega}} = \frac{\pi^2 g_\star}{30} \left(\frac{T^2}{T_{\text{end}}}\right)^4, \quad (3.28)$$

which turns out to be κ -independent. Therefore the DM freeze-out happens at

$$x_{\text{fo}} = \ln \left[\frac{3}{2} \sqrt{\frac{5}{\pi^5 g_\star}} g \frac{M_P \langle \sigma v \rangle T_{\text{end}}^2}{m} x_{\text{fo}}^{\frac{5}{2}} \right], \quad (3.29)$$

or equivalently

$$x_{\text{fo}} = -\frac{5}{2} W_{-1} \left[-\frac{2}{5} \left(\frac{3}{2} \sqrt{\frac{5}{\pi^5 g_\star}} g \frac{M_P \langle \sigma v \rangle T_{\text{end}}^2}{m} \right)^{-\frac{2}{5}} \right], \quad (3.30)$$

where W_{-1} is the -1 branch of the Lambert W function, and which is again independent on κ . Figure 4 shows the T_{end} dependence of x_{fo} as vertical lines.

3.1.4 Case 4: $T_{\text{fo}} \ll T_{\text{end}}$

This case corresponds to the scenario where $T_{\text{fo}} \ll T_{\text{end}}$. In this regime the non-standard cosmology has no effect on the final DM relic abundance, due to the fact that ϕ decays at a very high temperature, while the DM is still in chemical equilibrium with the SM thermal bath.

3.2 Varying the Particle Physics Parameters

Up to now we have studied the possibilities for reconstructing non-standard cosmologies after a DM detection assuming some given particle physics benchmarks. In this section we study the reconstruction prospects using different benchmarks both for the DM properties (m and $\langle \sigma v \rangle$), and the equation of state ω of ϕ .

Figure 5 shows the parameter space generating the observed DM abundance via the WIMP mechanism with non-standard cosmologies assuming $\omega = 0$ and different particle physics parameters. The left panel corresponds to $\langle \sigma v \rangle = 10^{-11} \text{ GeV}^{-2}$ and DM masses: $m = 10 \text{ GeV}$ (red), 100 GeV (blue) and 1 TeV (black). Notice that in this case, the colored bands corresponding to $\rho_\phi < \rho_R$ are different for each mass, because κ is defined at different scales ($T = m$). Additionally, the right panel depicts the cases where $m = 100 \text{ GeV}$ and $\langle \sigma v \rangle = 10^{-12} \text{ GeV}^{-2}$ (red), $10^{-11} \text{ GeV}^{-2}$ (blue) and $10^{-10} \text{ GeV}^{-2}$ (black). The gray bands correspond to $T_{\text{end}} < T_{\text{BBN}}$ and $\rho_\phi < \rho_R$. The behavior of the lines can be understood analytically. On the one hand, for low values of κ , we are in case 1 where the DM relic density scales like $\frac{T_{\text{end}}}{\langle \sigma v \rangle \kappa m}$ (up to a mild logarithmic dependence coming from x_{fo}), see eq. (3.8). Therefore, an increase of the DM mass or $\langle \sigma v \rangle$ decreases the final DM yield. This effect can be compensated by reducing the dilution factor D by either a rise of T_{end} or a decrease of κ . On the other hand, for high values of κ we are in case 3, where the DM relic density scales like $\frac{T_{\text{end}}^3}{\langle \sigma v \rangle m^4}$ (again up to a mild logarithmic dependence coming from x_{fo}), see eq. (3.25). As pointed out previously, this scenario is independent of κ . Therefore, an increase of either m or $\langle \sigma v \rangle$ has to be compensated by a rise of T_{end} .

Figure 6 presents in blue the parameter space compatible with the observed DM abundance via the WIMP mechanism with non-standard cosmologies, in the plane $[T_{\text{end}}, \kappa]$. We

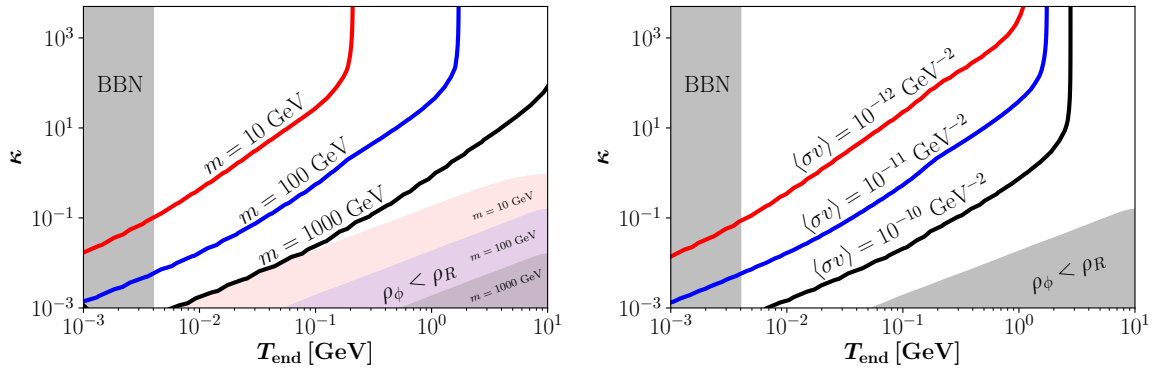


Figure 5. Parameter space generating the observed DM abundance via the WIMP mechanism with non-standard cosmologies, assuming $\omega = 0$ and different particle physics parameters. Left panel: $\langle\sigma v\rangle = 10^{-11} \text{ GeV}^{-2}$ and $m = 10 \text{ GeV}$ (red), 100 GeV (blue), and 1 TeV (black). The colored bands present the $\rho_\phi < \rho_R$ areas for $m = 10 \text{ GeV}$ (light red), 100 GeV (purple), and 1 TeV (gray). Right panel: $m = 100 \text{ GeV}$ and $\langle\sigma v\rangle = 10^{-12} \text{ GeV}^{-2}$ (red), $10^{-11} \text{ GeV}^{-2}$ (blue), and $10^{-10} \text{ GeV}^{-2}$ (black), while the gray right lower band correspond to $\rho_\phi < \rho_R$. The gray bands on the left correspond to $T_{\text{end}} < T_{\text{BBN}}$.

assumed $\omega = -2/3$ (upper left panel), $\omega = -1/3$ (upper right panel) and $\omega = +2/5$ (lower panel). For the particle physics benchmark we have chosen $m = 100 \text{ GeV}$ and $\langle\sigma v\rangle = 10^{-11} \text{ GeV}^{-2}$. The gray bands correspond to $T_{\text{end}} < T_{\text{BBN}}$ and $\rho_\phi < \rho_R$, while the fuchsia region for the $\omega = +2/5$ case shows the (semi-)relativistic freeze-out, i.e. $x_{\text{fo}} < 3$. The lines corresponding to $T_{\text{fo}} = T_{\text{eq}}$, $T_{\text{fo}} = T_c$ and $T_{\text{fo}} = T_{\text{end}}$ are overlaid.

On the left upper panel $\omega = -2/3$ corresponds to a ρ_ϕ that scales like a^{-1} . This implies that it gets diluted much slower than matter, and thus naturally dominates the total energy density of the Universe, even if its initial density is suppressed. One can therefore explore much lower values for κ , compared to the case $\omega = 0$ in fig. 2, without violating the BBN bound. As expected from the analytical estimations, in the regions $T_{\text{eq}} \ll T_{\text{fo}}$ (case 1) and $T_c \ll T_{\text{fo}} \ll T_{\text{eq}}$ (case 2), κ scales like T_{end}^3 and $T_{\text{end}}^{18/5}$, respectively. Also, when $T_{\text{end}} \ll T_{\text{fo}} \ll T_c$ (case 3) the DM yield is independent on κ . In the right lower corner the ρ_ϕ is always subdominant with respect to radiation, and hence corresponds to the usual case, radiation dominated.

Similarly, on the right upper panel $\omega = -1/3$ corresponds to a ρ_ϕ that scales like a^{-2} . In the regions $T_{\text{eq}} \ll T_{\text{fo}}$ (case 1) and $T_c \ll T_{\text{fo}} \ll T_{\text{eq}}$ (case 2), κ scales like T_{end}^2 and T_{end}^3 , respectively. Also, when $T_{\text{end}} \ll T_{\text{fo}} \ll T_c$ (case 3) the DM yield is independent on κ .

On contrary, the lower panel corresponds to $\omega = +2/5$ and hence $\rho_\phi \propto a^{-21/5}$. The ϕ energy density gets diluted much faster than matter (and radiation) and therefore very large values for κ are needed to compensate. In turn, large values of κ boost the Hubble expansion rate implying a much earlier freeze-out. The upper left region corresponds to $x_{\text{fo}} < 3$, yielding a (semi-)relativistic freeze-out which is incompatible with our approximations. In this case with $\omega > 1/3$ and $\kappa \gg 1$, T_{eq} is not defined, as $\rho_\phi = \rho_R$ only happens when ϕ decays, implying that the case 1 is never realized. Additionally, in the case 2, $\kappa \propto T_{\text{end}}^{-2/3}$ and in the case 3 the DM yield is again independent of κ .

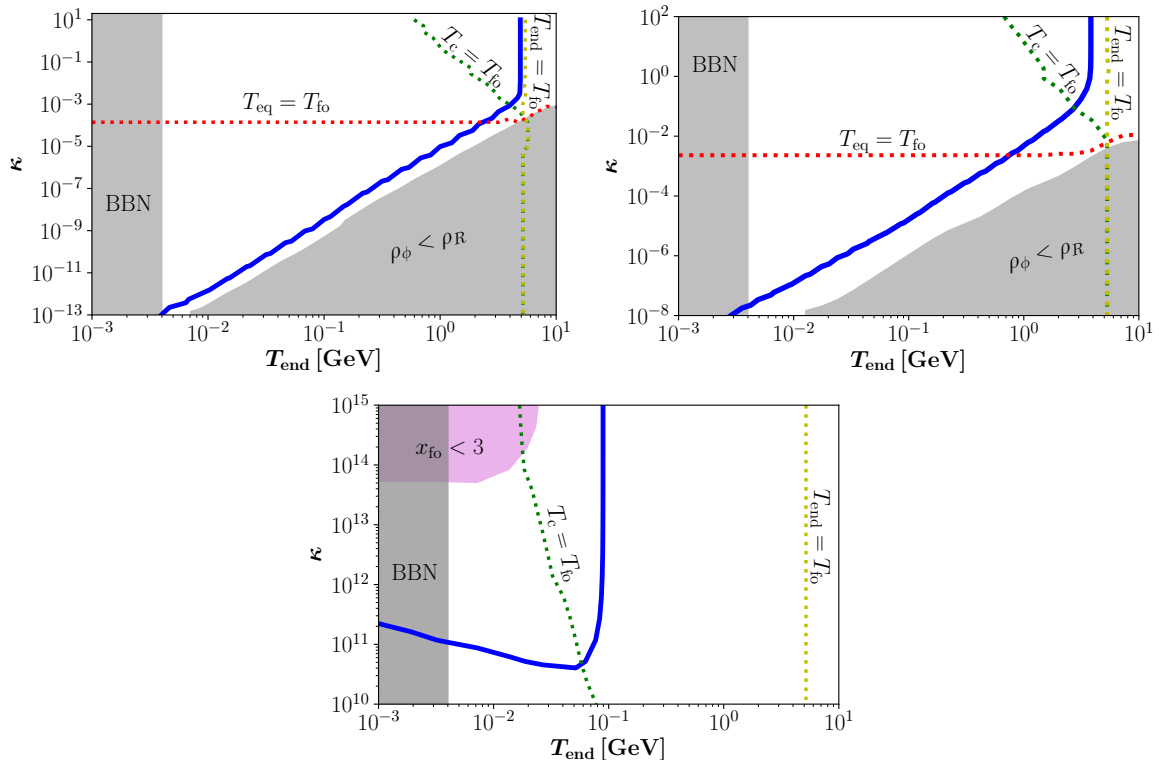


Figure 6. Parameter space generating the observed DM abundance via the WIMP mechanism with non-standard cosmologies, assuming $\omega = -2/3$ (upper left panel), $\omega = -1/3$ (upper right panel) and $\omega = +2/5$ (lower panel). For the particle physics benchmark we have taken $m = 100$ GeV and $\langle\sigma v\rangle = 10^{-11}$ GeV $^{-2}$. The gray bands correspond to $T_{\text{end}} < T_{\text{BBN}}$ and $\rho_\phi < \rho_R$, while the fuchsia region for the $\omega = +2/5$ case shows the (semi)-relativistic freeze-out. The lines corresponding to $T_{\text{fo}} = T_{\text{eq}}$, $T_{\text{fo}} = T_c$ and $T_{\text{fo}} = T_{\text{end}}$ are overlaid.

3.3 Varying the Non-standard Cosmological Parameters

In this section we study the impact of the non-standard cosmology on the particle physics parameter space $[m, \langle\sigma v\rangle]$.

Figure 7 shows in blue the particle physics parameter space $[m, \langle\sigma v\rangle]$ that gives rise to the observed DM abundance, for fixed non-standard cosmologies, $T_{\text{end}} = 7 \times 10^{-3}$ GeV and $\kappa = 10^{-2}$ (upper left panel), $T_{\text{end}} = 10^{-1}$ GeV and $\kappa = 1$ (upper right panel), and $T_{\text{end}} = 2$ GeV and $\kappa = 10^3$ (lower panel), assuming $\omega = 0$. The black line, for which $\langle\sigma v\rangle = \langle\sigma v\rangle_0$, shows the thermally averaged cross sections needed to have a WIMP production with standard cosmology. The small variations are due to the changes of the number of relativistic degrees of freedom g_\star and $g_{\star S}$ [73]. Larger cross sections (in gray) are incompatible with the WIMP mechanism, even in the cases of non-standard cosmologies. The red, yellow and black markers correspond to the benchmark points shown in fig. 2. The dotted lines corresponding to $T_{\text{fo}} = T_c$ (green) and $T_{\text{fo}} = T_{\text{end}}$ (yellow) are overlaid. In the upper left panel ($T_{\text{end}} = 7 \times 10^{-3}$ GeV and $\kappa = 10^{-2}$) the gray band on the left corresponds to $\rho_R > \rho_\phi$, i.e. the limit of standard cosmology. That panel correspond to the case 1, where $T_{\text{eq}} < T_{\text{fo}}$. In order to keep a constant DM relic abundance, in eq. (3.8)

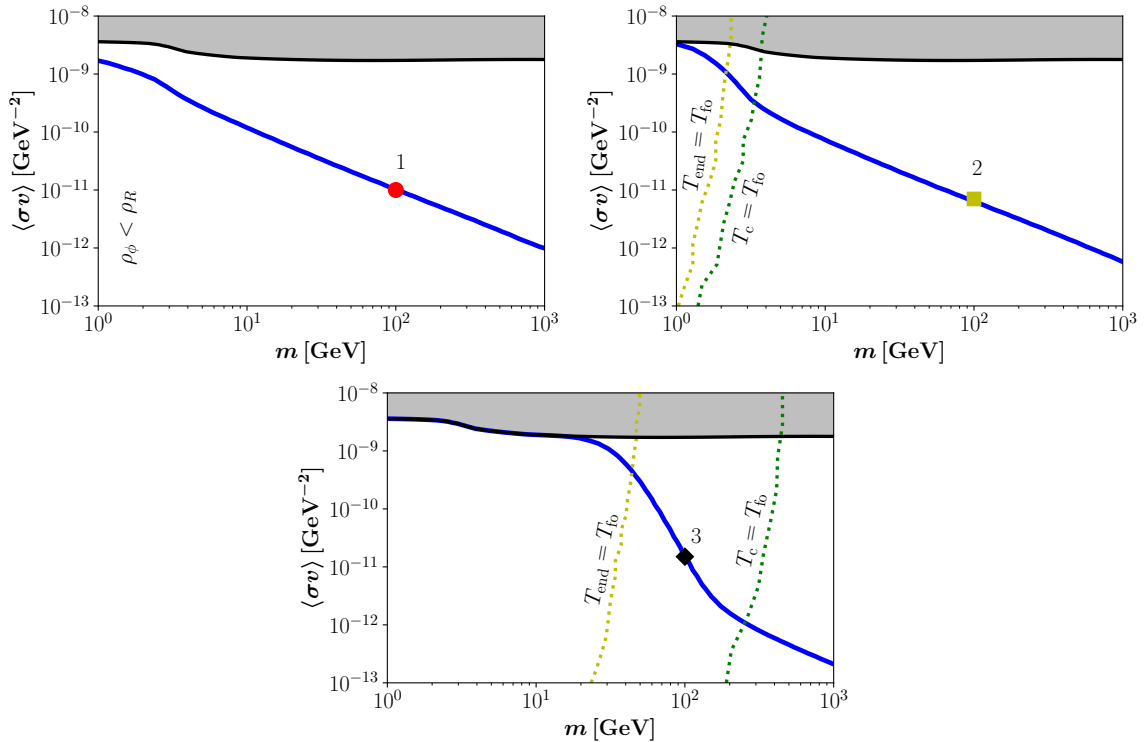


Figure 7. Parameter space (in blue) that reproduces the observed DM abundance via the WIMP mechanism, assuming $T_{\text{end}} = 7 \times 10^{-3}$ GeV and $\kappa = 10^{-2}$ (upper left panel), $T_{\text{end}} = 10^{-1}$ GeV and $\kappa = 1$ (upper right panel), and $T_{\text{end}} = 2$ GeV and $\kappa = 10^3$ (lower panel), for $\omega = 0$. The red, yellow and black markers correspond to the benchmark points shown in fig. 2. The black line ($\langle\sigma v\rangle = \langle\sigma v\rangle_0$) shows the cross sections needed to have a WIMP production with standard cosmology. Larger cross sections (in gray) are incompatible with the WIMP mechanism, even in the cases of non-standard cosmologies. The lines corresponding to $T_{\text{fo}} = T_c$ and $T_{\text{fo}} = T_{\text{end}}$ are overlaid.

$m \times Y_{\text{obs}}$ has to stay constant as well. That implies that $\langle\sigma v\rangle \propto m^{\frac{3\omega-1}{1+\omega}}$, which translates to $\langle\sigma v\rangle \propto 1/m$ for $\omega = 0$.

A similar behavior appears in the upper right and lower panels, when $T_c \ll T_{\text{fo}} \ll T_{\text{eq}}$ (case 2), which corresponds to high masses, to the right of the dotted green lines: $\langle\sigma v\rangle \propto m^{\frac{3\omega-1}{1+\omega}}$, see eq. (3.15). For $\omega = 0$ it translates to $\langle\sigma v\rangle \propto m^{-1}$. However, for intermediate masses, between the yellow and the green lines (i.e. for $T_{\text{end}} \ll T_{\text{fo}} \ll T_c$), case 3 happens. In that scenario, for keeping constant the DM relic abundance $\langle\sigma v\rangle \propto m^{\frac{5\omega-3}{1+\omega}}$, which for $\omega = 0$ implies $\langle\sigma v\rangle \propto m^{-3}$, see eq. (3.25). Finally, for low masses, to the left of the dotted yellow lines $T_{\text{fo}} < T_{\text{end}}$, and therefore the cross section needed to have a successful WIMP DM production is the usual $\langle\sigma v\rangle_0$, characteristic of the standard cosmology (case 4).

Figure 8 depicts in white the particle physics parameter space $[m, \langle\sigma v\rangle]$ that could reproduce the observed DM abundance via the WIMP mechanism with non-standard cosmologies, assuming $\omega = 0$. The case $\langle\sigma v\rangle = \langle\sigma v\rangle_0 = \text{few} \times 10^{-9} \text{ GeV}^{-2}$ giving rise to the simplest WIMP mechanism with the standard cosmology is also shown with a thick black line. The gray regions show the areas where different cosmologies can not conciliate a DM with mass m and cross-section $\langle\sigma v\rangle$ with the WIMP paradigm. On the one hand, the case $\omega = 0$ can only dilute

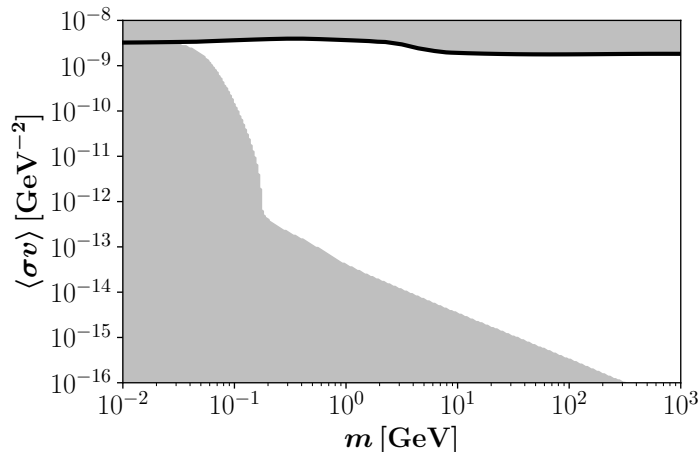


Figure 8. Parameter space (in white) that could reproduce the observed DM abundance via the WIMP mechanism with non-standard cosmologies, assuming $\omega = 0$. For completeness we also show the standard cosmological scenario with $\langle\sigma v\rangle = \langle\sigma v\rangle_0$ with a thick black line.

the DM abundance, which means that cross sections higher than $\langle\sigma v\rangle_0$ can not become viable (upper gray region). On the other hand, a large part of the parameter space $\langle\sigma v\rangle < \langle\sigma v\rangle_0$ (in white) becomes compatible with the WIMP mechanism. However, the observed DM relic abundance can not be reproduced for arbitrarily small values for $\langle\sigma v\rangle$ without reaching the (semi-)relativistic freeze-out limit, $x_{\text{fo}} < 3$ (lower gray region). For masses $m \gtrsim 300$ MeV, the bound corresponds to the case 2, and can be analytically understood by the use of eqs. (3.13) and (3.15):

$$\langle\sigma v\rangle = \left[\frac{45(1-\omega)}{4\pi\sqrt{10g_*}} \frac{1}{M_P Y_{\text{obs}} m} \right]^{\frac{1+\omega}{2}} \left[\frac{2}{3g} \sqrt{\frac{\pi^5 g_*}{5}} \frac{x_{\text{fo}}^{\frac{3}{2}} e^{x_{\text{fo}}}}{M_P} \right]^{\frac{1-\omega}{2}} \frac{T_{\text{end}}^{\frac{1-3\omega}{2}}}{m^{1-2\omega}}, \quad (3.31)$$

that for $\omega = 0$ gives $\langle\sigma v\rangle \propto m^{-1}$, and takes the minimum allowed value when $x_{\text{fo}} = 3$ and $T_{\text{end}} = T_{\text{BBN}}$. Likewise, for 10 MeV $\lesssim m \lesssim 300$ MeV the bound comes from case 3. Equation (3.25) can be rewritten as

$$\langle\sigma v\rangle = \frac{45}{4\pi\sqrt{10g_*}} \frac{1-\omega}{M_P Y_{\text{obs}} m} x_{\text{fo}}^{4\frac{1-\omega}{1+\omega}} \left(\frac{T_{\text{end}}}{m} \right)^{\frac{3-5\omega}{1+\omega}}, \quad (3.32)$$

which again represents a lower bound when taking $T_{\text{end}} = T_{\text{BBN}}$ and x_{fo} as given in eq. (3.30). From fig. 8 one can see that DM lighter than ~ 30 MeV can only be produced in the standard cosmological scenario with $\langle\sigma v\rangle = \langle\sigma v\rangle_0$. For those masses, our non-standard cosmological setup with $\omega = 0$ can not conciliate smaller cross sections with the WIMP mechanism.

Before closing this section we would like to emphasize that in this work the thermally averaged cross section $\langle\sigma v\rangle$ is evaluated at freeze-out, i.e. when DM velocity is $v \simeq 1/3$. There are bounds at much lower redshifts coming from CMB [113], the galactic center [114] and dwarfs galaxies [115]. However these bounds depend on the velocity scaling of $\langle\sigma v\rangle$ and, in this model independent approach, can not be applied directly.

4 Conclusions

Despite the large amount of searches over the past decades, dark matter (DM) has not been found. In particular, scenarios where DM is a weakly interacting massive particle (WIMP) have received by far the biggest attention both theoretically and experimentally, but unfortunately there is no overwhelming evidence of WIMP DM. A simple reason for this might be that the cosmological history was non-standard at early times, which affects the typical DM interaction rates, reducing the naively expected annihilation cross sections.

In this paper we considered the production of WIMP DM in the early Universe following a particle physics model independent way, where the DM dynamics is fully parametrized by its mass m and its total thermally averaged annihilation cross section $\langle\sigma v\rangle$. Additionally, we studied scenarios where for some period the expansion of the Universe was governed by a component ϕ with an effective equation of state $\omega = p_\phi/\rho_\phi$, where p_ϕ is its pressure and ρ_ϕ its energy density.

Once DM is discovered and its particle physics properties have been reconstructed, a major question rises concerning the DM production mechanism. If the inferred value of $\langle\sigma v\rangle$ is in the ballpark of $\text{few}\times 10^{-26} \text{ cm}^3/\text{s}$, the simpler freeze-out mechanism with a standard cosmology will be strongly favored. However, if that turns out not to be the case, one can either look for different DM production mechanisms or for alternative cosmological scenarios. The latter option was pursued in this study.

A detailed analysis was performed both numerically and analytically, by solving the system of coupled Boltzmann equations. Different regimes have been found, characterized by the temperature at which the DM freeze-out happens compared to the proper scales of the non-standard cosmology. We studied the effects of varying both the particles physics and the non-standard cosmological parameters, and found the parameter space that was compatible with the observed DM abundance via the WIMP paradigm.

We found that large regions of the particle physics parameter space can be reconciled with the WIMP paradigm in the case of non-standard cosmologies for DM heavier than $\sim 30 \text{ MeV}$. An effect on the genesis of lighter WIMP DM without modifying the usual BBN dynamics is not possible within our approach. On the contrary, heavy DM WIMP can be compatible with the WIMP mechanism and cross sections much smaller than the canonical $\langle\sigma v\rangle_0 = \text{few}\times 10^{-9} \text{ GeV}^{-2}$. In particular, for TeV DM one can go to values as small as $\langle\sigma v\rangle \simeq 3 \times 10^{-17} \text{ GeV}^{-2} \sim 3 \times 10^{-34} \text{ cm}^3/\text{s}$.

Acknowledgments

We would like to thank Fazlollah Hajkarim and Sergio Palomares-Ruiz for valuable discussions. NB is partially supported by Spanish MINECO under Grant FPA2017-84543-P. AH acknowledges the Joven Investigador program by Universidad Antonio Nariño. This project has received funding from the European Union's Horizon 2020 research and innovation programme under the Marie Skłodowska-Curie grant agreements 674896 and 690575, and from Universidad Antonio Nariño grants 2017239, 2018204, 2019101 and 2019248. CM is supported by CONICYT- PCHA/Doctorado Nacional/2018-21180309. PA and CM are supported by FONDECYT Project 1161150. This research made use of IPython [116], Matplotlib [117] and SciPy [118].

References

- [1] PLANCK collaboration, *Planck 2018 results. VI. Cosmological parameters*, [1807.06209](#).
- [2] G. Bertone, D. Hooper and J. Silk, *Particle dark matter: Evidence, candidates and constraints*, *Phys. Rept.* **405** (2005) 279 [[hep-ph/0404175](#)].
- [3] G. Arcadi, M. Dutra, P. Ghosh, M. Lindner, Y. Mambrini, M. Pierre et al., *The waning of the WIMP? A review of models, searches, and constraints*, *Eur. Phys. J.* **C78** (2018) 203 [[1703.07364](#)].
- [4] T. Lin, *Dark matter models and direct detection*, *PoS* **333** (2019) 009 [[1904.07915](#)].
- [5] D. Hooper, *TASI Lectures on Indirect Searches For Dark Matter*, *PoS TASI2018* (2019) 010 [[1812.02029](#)].
- [6] J. McDonald, *Thermally generated gauge singlet scalars as selfinteracting dark matter*, *Phys.Rev.Lett.* **88** (2002) 091304 [[hep-ph/0106249](#)].
- [7] K.-Y. Choi and L. Roszkowski, *E-WIMPs*, *AIP Conf. Proc.* **805** (2006) 30 [[hep-ph/0511003](#)].
- [8] A. Kusenko, *Sterile neutrinos, dark matter, and the pulsar velocities in models with a Higgs singlet*, *Phys. Rev. Lett.* **97** (2006) 241301 [[hep-ph/0609081](#)].
- [9] K. Petraki and A. Kusenko, *Dark-matter sterile neutrinos in models with a gauge singlet in the Higgs sector*, *Phys. Rev.* **D77** (2008) 065014 [[0711.4646](#)].
- [10] L. J. Hall, K. Jedamzik, J. March-Russell and S. M. West, *Freeze-In Production of FIMP Dark Matter*, *JHEP* **1003** (2010) 080 [[0911.1120](#)].
- [11] X. Chu, T. Hambye and M. H. G. Tytgat, *The Four Basic Ways of Creating Dark Matter Through a Portal*, *JCAP* **1205** (2012) 034 [[1112.0493](#)].
- [12] G. Bélanger, F. Boudjema, A. Goudelis, A. Pukhov and B. Zaldivar, *micrOMEGAs5.0 : Freeze-in*, *Comput. Phys. Commun.* **231** (2018) 173 [[1801.03509](#)].
- [13] N. Bernal, M. Heikinheimo, T. Tenkanen, K. Tuominen and V. Vaskonen, *The Dawn of FIMP Dark Matter: A Review of Models and Constraints*, *Int. J. Mod. Phys.* **A32** (2017) 1730023 [[1706.07442](#)].
- [14] S. Davidson, M. Losada and A. Riotto, *A New perspective on baryogenesis*, *Phys. Rev. Lett.* **84** (2000) 4284 [[hep-ph/0001301](#)].
- [15] G. F. Giudice, E. W. Kolb and A. Riotto, *Largest temperature of the radiation era and its cosmological implications*, *Phys. Rev.* **D64** (2001) 023508 [[hep-ph/0005123](#)].
- [16] R. Allahverdi, B. Dutta and K. Sinha, *Baryogenesis and Late-Decaying Moduli*, *Phys. Rev.* **D82** (2010) 035004 [[1005.2804](#)].
- [17] A. Beniwal, M. Lewicki, J. D. Wells, M. White and A. G. Williams, *Gravitational wave, collider and dark matter signals from a scalar singlet electroweak baryogenesis*, *JHEP* **08** (2017) 108 [[1702.06124](#)].
- [18] R. Allahverdi, P. S. B. Dev and B. Dutta, *A simple testable model of baryon number violation: Baryogenesis, dark matter, neutron-antineutron oscillation and collider signals*, *Phys. Lett.* **B779** (2018) 262 [[1712.02713](#)].
- [19] N. Bernal and C. S. Fong, *Hot Leptogenesis from Thermal Dark Matter*, *JCAP* **1710** (2017) 042 [[1707.02988](#)].
- [20] H. Assadullahi and D. Wands, *Gravitational waves from an early matter era*, *Phys. Rev.* **D79** (2009) 083511 [[0901.0989](#)].
- [21] R. Durrer and J. Hasenkamp, *Testing Superstring Theories with Gravitational Waves*, *Phys. Rev.* **D84** (2011) 064027 [[1105.5283](#)].

- [22] L. Alabidi, K. Kohri, M. Sasaki and Y. Sendouda, *Observable induced gravitational waves from an early matter phase*, *JCAP* **1305** (2013) 033 [[1303.4519](#)].
- [23] F. D’Eramo and K. Schmitz, *Imprint of a scalar era on the primordial spectrum of gravitational waves*, [1904.07870](#).
- [24] N. Bernal and F. Hajkarim, *Primordial Gravitational Waves in Nonstandard Cosmologies*, *Phys. Rev.* **D100** (2019) 063502 [[1905.10410](#)].
- [25] D. G. Figueroa and E. H. Tanin, *Ability of LIGO and LISA to probe the equation of state of the early Universe*, *JCAP* **2019** (2020) 011 [[1905.11960](#)].
- [26] J. D. Barrow, *Massive Particles as a Probe of the Early Universe*, *Nucl. Phys.* **B208** (1982) 501.
- [27] L. H. Ford, *Gravitational Particle Creation and Inflation*, *Phys. Rev.* **D35** (1987) 2955.
- [28] G. Kane, K. Sinha and S. Watson, *Cosmological Moduli and the Post-Inflationary Universe: A Critical Review*, *Int. J. Mod. Phys.* **D24** (2015) 1530022 [[1502.07746](#)].
- [29] R. T. Co, F. D’Eramo, L. J. Hall and D. Pappadopulo, *Freeze-In Dark Matter with Displaced Signatures at Colliders*, *JCAP* **1512** (2015) 024 [[1506.07532](#)].
- [30] H. Davoudiasl, D. Hooper and S. D. McDermott, *Inflatable Dark Matter*, *Phys. Rev. Lett.* **116** (2016) 031303 [[1507.08660](#)].
- [31] L. Randall, J. Scholtz and J. Unwin, *Flooded Dark Matter and S Level Rise*, *JHEP* **03** (2016) 011 [[1509.08477](#)].
- [32] A. Berlin, D. Hooper and G. Krnjaic, *PeV-Scale Dark Matter as a Thermal Relic of a Decoupled Sector*, *Phys. Lett.* **B760** (2016) 106 [[1602.08490](#)].
- [33] T. Tenkanen and V. Vaskonen, *Reheating the Standard Model from a hidden sector*, *Phys. Rev.* **D94** (2016) 083516 [[1606.00192](#)].
- [34] J. A. Dror, E. Kuflik and W. H. Ng, *Codecaying Dark Matter*, *Phys. Rev. Lett.* **117** (2016) 211801 [[1607.03110](#)].
- [35] A. Berlin, D. Hooper and G. Krnjaic, *Thermal Dark Matter From A Highly Decoupled Sector*, *Phys. Rev.* **D94** (2016) 095019 [[1609.02555](#)].
- [36] F. D’Eramo, N. Fernandez and S. Profumo, *When the Universe Expands Too Fast: Relentless Dark Matter*, *JCAP* **1705** (2017) 012 [[1703.04793](#)].
- [37] S. Hamdan and J. Unwin, *Dark Matter Freeze-out During Matter Domination*, *Mod. Phys. Lett.* **A33** (2018) 1850181 [[1710.03758](#)].
- [38] L. Visinelli, *(Non-)thermal production of WIMPs during kination*, *Symmetry* **10** (2018) 546 [[1710.11006](#)].
- [39] J. A. Dror, E. Kuflik, B. Melcher and S. Watson, *Concentrated Dark Matter: Enhanced Small-scale Structure from Co-Decaying Dark Matter*, *Phys. Rev.* **D97** (2018) 063524 [[1711.04773](#)].
- [40] M. Drees and F. Hajkarim, *Dark Matter Production in an Early Matter Dominated Era*, *JCAP* **1802** (2018) 057 [[1711.05007](#)].
- [41] F. D’Eramo, N. Fernandez and S. Profumo, *Dark Matter Freeze-in Production in Fast-Expanding Universes*, *JCAP* **1802** (2018) 046 [[1712.07453](#)].
- [42] D. Maity and P. Saha, *Connecting CMB anisotropy and cold dark matter phenomenology via reheating*, *Phys. Rev.* **D98** (2018) 103525 [[1801.03059](#)].
- [43] N. Bernal, C. Cosme and T. Tenkanen, *Phenomenology of Self-Interacting Dark Matter in a Matter-Dominated Universe*, *Eur. Phys. J.* **C79** (2019) 99 [[1803.08064](#)].

- [44] E. Hardy, *Higgs portal dark matter in non-standard cosmological histories*, *JHEP* **06** (2018) 043 [[1804.06783](#)].
- [45] D. Maity and P. Saha, *CMB constraints on dark matter phenomenology via reheating in Minimal plateau inflation*, *Phys. Dark Univ.* (2018) 100317 [[1804.10115](#)].
- [46] T. Hambye, A. Strumia and D. Teresi, *Super-cool Dark Matter*, *JHEP* **08** (2018) 188 [[1805.01473](#)].
- [47] N. Bernal, C. Cosme, T. Tenkanen and V. Vaskonen, *Scalar singlet dark matter in non-standard cosmologies*, *Eur. Phys. J.* **C79** (2019) 30 [[1806.11122](#)].
- [48] A. Arbey, J. Ellis, F. Mahmoudi and G. Robbins, *Dark Matter Casts Light on the Early Universe*, *JHEP* **10** (2018) 132 [[1807.00554](#)].
- [49] M. Drees and F. Hajkarim, *Neutralino Dark Matter in Scenarios with Early Matter Domination*, *JHEP* **12** (2018) 042 [[1808.05706](#)].
- [50] A. Betancur and Ó. Zapata, *Phenomenology of doublet-triplet fermionic dark matter in nonstandard cosmology and multicomponent dark sectors*, *Phys. Rev.* **D98** (2018) 095003 [[1809.04990](#)].
- [51] C. Maldonado and J. Unwin, *Establishing the Dark Matter Relic Density in an Era of Particle Decays*, *JCAP* **1906** (2019) 037 [[1902.10746](#)].
- [52] A. Poulin, *Dark matter freeze-out in modified cosmological scenarios*, *Phys. Rev.* **D100** (2019) 043022 [[1905.03126](#)].
- [53] T. Tenkanen, *The Standard Model Higgs and Hidden Sector Cosmology*, [1905.11737](#).
- [54] M. Kamionkowski and M. S. Turner, *Thermal Relics: Do we Know their Abundances?*, *Phys. Rev.* **D42** (1990) 3310.
- [55] J. McDonald, *WIMP Densities in Decaying Particle Dominated Cosmology*, *Phys. Rev.* **D43** (1991) 1063.
- [56] P. Salati, *Quintessence and the relic density of neutralinos*, *Phys. Lett.* **B571** (2003) 121 [[astro-ph/0207396](#)].
- [57] D. Comelli, M. Pietroni and A. Riotto, *Dark energy and dark matter*, *Phys. Lett.* **B571** (2003) 115 [[hep-ph/0302080](#)].
- [58] F. Rosati, *Quintessential enhancement of dark matter abundance*, *Phys. Lett.* **B570** (2003) 5 [[hep-ph/0302159](#)].
- [59] C. Pallis, *Massive particle decay and cold dark matter abundance*, *Astropart. Phys.* **21** (2004) 689 [[hep-ph/0402033](#)].
- [60] G. B. Gelmini and P. Gondolo, *Neutralino with the right cold dark matter abundance in (almost) any supersymmetric model*, *Phys. Rev.* **D74** (2006) 023510 [[hep-ph/0602230](#)].
- [61] G. Gelmini, P. Gondolo, A. Soldatenko and C. E. Yaguna, *The Effect of a late decaying scalar on the neutralino relic density*, *Phys. Rev.* **D74** (2006) 083514 [[hep-ph/0605016](#)].
- [62] A. Arbey and F. Mahmoudi, *SUSY constraints from relic density: High sensitivity to pre-BBN expansion rate*, *Phys. Lett.* **B669** (2008) 46 [[0803.0741](#)].
- [63] T. Cohen, D. E. Morrissey and A. Pierce, *Changes in Dark Matter Properties After Freeze-Out*, *Phys. Rev.* **D78** (2008) 111701 [[0808.3994](#)].
- [64] A. Arbey and F. Mahmoudi, *SUSY Constraints, Relic Density, and Very Early Universe*, *JHEP* **05** (2010) 051 [[0906.0368](#)].
- [65] D. J. H. Chung, E. W. Kolb and A. Riotto, *Production of massive particles during reheating*, *Phys. Rev.* **D60** (1999) 063504 [[hep-ph/9809453](#)].

- [66] E. W. Kolb, A. Notari and A. Riotto, *On the reheating stage after inflation*, *Phys. Rev.* **D68** (2003) 123505 [[hep-ph/0307241](#)].
- [67] M. A. G. Garcia, Y. Mambrini, K. A. Olive and M. Peloso, *Enhancement of the Dark Matter Abundance Before Reheating: Applications to Gravitino Dark Matter*, *Phys. Rev.* **D96** (2017) 103510 [[1709.01549](#)].
- [68] J. Ellis, M. A. G. Garcia, D. V. Nanopoulos, K. A. Olive and M. Peloso, *Post-Inflationary Gravitino Production Revisited*, *JCAP* **1603** (2016) 008 [[1512.05701](#)].
- [69] G. B. Gelmini and P. Gondolo, *Ultra-cold WIMPs: relics of non-standard pre-BBN cosmologies*, *JCAP* **0810** (2008) 002 [[0803.2349](#)].
- [70] L. Visinelli and P. Gondolo, *Kinetic decoupling of WIMPs: analytic expressions*, *Phys. Rev.* **D91** (2015) 083526 [[1501.02233](#)].
- [71] I. R. Waldstein, A. L. Erickcek and C. Ilie, *Quasidecoupled state for dark matter in nonstandard thermal histories*, *Phys. Rev.* **D95** (2017) 123531 [[1609.05927](#)].
- [72] I. R. Waldstein and A. L. Erickcek, *Comment on “Kinetic decoupling of WIMPs: Analytic expressions”*, *Phys. Rev.* **D95** (2017) 088301 [[1707.03417](#)].
- [73] G. Steigman, B. Dasgupta and J. F. Beacom, *Precise Relic WIMP Abundance and its Impact on Searches for Dark Matter Annihilation*, *Phys. Rev.* **D86** (2012) 023506 [[1204.3622](#)].
- [74] O. Mena, S. Palomares-Ruiz and S. Pascoli, *Reconstructing WIMP properties with neutrino detectors*, *Phys. Lett.* **B664** (2008) 92 [[0706.3909](#)].
- [75] M. Drees and C.-L. Shan, *Model-Independent Determination of the WIMP Mass from Direct Dark Matter Detection Data*, *JCAP* **0806** (2008) 012 [[0803.4477](#)].
- [76] N. Bernal, A. Goudelis, Y. Mambrini and C. Muñoz, *Determining the WIMP mass using the complementarity between direct and indirect searches and the ILC*, *JCAP* **0901** (2009) 046 [[0804.1976](#)].
- [77] N. Bernal, *WIMP mass from direct, indirect dark matter detection experiments and colliders: A Complementary and model-independent approach*, in *Proceedings, 43rd Rencontres de Moriond on Electroweak Interactions and Unified Theories: La Thuile, Italy, March 1-8, 2008*, 2008, [0805.2241](#), <https://inspirehep.net/record/785807/files/arXiv:0805.2241.pdf>.
- [78] L. Bergström, T. Bringmann and J. Edsjö, *Complementarity of direct dark matter detection and indirect detection through gamma-rays*, *Phys. Rev.* **D83** (2011) 045024 [[1011.4514](#)].
- [79] M. Pato, L. Baudis, G. Bertone, R. Ruiz de Austri, L. E. Strigari and R. Trotta, *Complementarity of Dark Matter Direct Detection Targets*, *Phys. Rev.* **D83** (2011) 083505 [[1012.3458](#)].
- [80] K. Arisaka et al., *Studies of a three-stage dark matter and neutrino observatory based on multi-ton combinations of liquid xenon and liquid argon detectors*, *Astropart. Phys.* **36** (2012) 93 [[1107.1295](#)].
- [81] D. G. Cerdeño et al., *Complementarity of dark matter direct detection: the role of bolometric targets*, *JCAP* **1307** (2013) 028 [[1304.1758](#)].
- [82] C. Arina, G. Bertone and H. Silverwood, *Complementarity of direct and indirect Dark Matter detection experiments*, *Phys. Rev.* **D88** (2013) 013002 [[1304.5119](#)].
- [83] A. H. G. Peter, V. Gluscevic, A. M. Green, B. J. Kavanagh and S. K. Lee, *WIMP physics with ensembles of direct-detection experiments*, *Phys. Dark Univ.* **5-6** (2014) 45 [[1310.7039](#)].
- [84] B. J. Kavanagh, M. Fornasa and A. M. Green, *Probing WIMP particle physics and astrophysics with direct detection and neutrino telescope data*, *Phys. Rev.* **D91** (2015) 103533 [[1410.8051](#)].

- [85] L. Roszkowski, E. M. Sessolo, S. Trojanowski and A. J. Williams, *Reconstructing WIMP properties through an interplay of signal measurements in direct detection, Fermi-LAT, and CTA searches for dark matter*, *JCAP* **1608** (2016) 033 [[1603.06519](#)].
- [86] F. S. Queiroz, W. Rodejohann and C. E. Yaguna, *Is the dark matter particle its own antiparticle?*, *Phys. Rev.* **D95** (2017) 095010 [[1610.06581](#)].
- [87] L. Roszkowski, S. Trojanowski and K. Turzyński, *Towards understanding thermal history of the Universe through direct and indirect detection of dark matter*, *JCAP* **1710** (2017) 005 [[1703.00841](#)].
- [88] B. J. Kavanagh, F. S. Queiroz, W. Rodejohann and C. E. Yaguna, *Prospects for determining the particle/antiparticle nature of WIMP dark matter with direct detection experiments*, *JHEP* **10** (2017) 059 [[1706.07819](#)].
- [89] G. Bertone, N. Bozorgnia, J. S. Kim, S. Liem, C. McCabe, S. Otten et al., *Identifying WIMP dark matter from particle and astroparticle data*, *JCAP* **1803** (2018) 026 [[1712.04793](#)].
- [90] F. S. Queiroz and C. E. Yaguna, *Gamma-ray lines may reveal the CP nature of the dark matter particle*, *JCAP* **1901** (2019) 047 [[1810.07068](#)].
- [91] A. M. Green, *Effect of halo modeling on WIMP exclusion limits*, *Phys. Rev.* **D66** (2002) 083003 [[astro-ph/0207366](#)].
- [92] M. Zemp, J. Diemand, M. Kuhlen, P. Madau, B. Moore, D. Potter et al., *The Graininess of Dark Matter Haloes*, *Mon. Not. Roy. Astron. Soc.* **394** (2009) 641 [[0812.2033](#)].
- [93] C. McCabe, *The Astrophysical Uncertainties Of Dark Matter Direct Detection Experiments*, *Phys. Rev.* **D82** (2010) 023530 [[1005.0579](#)].
- [94] N. Bernal and S. Palomares-Ruiz, *Constraining Dark Matter Properties with Gamma-Rays from the Galactic Center with Fermi-LAT*, *Nucl. Phys.* **B857** (2012) 380 [[1006.0477](#)].
- [95] M. Pato, O. Agertz, G. Bertone, B. Moore and R. Teyssier, *Systematic uncertainties in the determination of the local dark matter density*, *Phys. Rev.* **D82** (2010) 023531 [[1006.1322](#)].
- [96] N. Bernal and S. Palomares-Ruiz, *Constraining the Milky Way Dark Matter Density Profile with Gamma-Rays with Fermi-LAT*, *JCAP* **1201** (2012) 006 [[1103.2377](#)].
- [97] M. Fairbairn, T. Douce and J. Swift, *Quantifying Astrophysical Uncertainties on Dark Matter Direct Detection Results*, *Astropart. Phys.* **47** (2013) 45 [[1206.2693](#)].
- [98] N. Bernal, J. E. Forero-Romero, R. Garani and S. Palomares-Ruiz, *Systematic uncertainties from halo asphericity in dark matter searches*, *JCAP* **1409** (2014) 004 [[1405.6240](#)].
- [99] N. Bernal, J. E. Forero-Romero, R. Garani and S. Palomares-Ruiz, *Systematic uncertainties from halo asphericity in dark matter searches*, *Nucl. Part. Phys. Proc.* **267-269** (2015) 345.
- [100] N. Bernal, L. Necib and T. R. Slatyer, *Spherical Cows in Dark Matter Indirect Detection*, *JCAP* **1612** (2016) 030 [[1606.00433](#)].
- [101] M. Benito, N. Bernal, N. Bozorgnia, F. Calore and F. Iocco, *Particle Dark Matter Constraints: the Effect of Galactic Uncertainties*, *JCAP* **1702** (2017) 007 [[1612.02010](#)].
- [102] A. M. Green, *Astrophysical uncertainties on the local dark matter distribution and direct detection experiments*, *J. Phys.* **G44** (2017) 084001 [[1703.10102](#)].
- [103] A. Ibarra, B. J. Kavanagh and A. Rappelt, *Bracketing the impact of astrophysical uncertainties on local dark matter searches*, *JCAP* **1812** (2018) 018 [[1806.08714](#)].
- [104] M. Benito, A. Cuoco and F. Iocco, *Handling the Uncertainties in the Galactic Dark Matter Distribution for Particle Dark Matter Searches*, *JCAP* **1903** (2019) 033 [[1901.02460](#)].
- [105] E. V. Karukes, M. Benito, F. Iocco, R. Trotta and A. Geringer-Sameth, *Bayesian reconstruction of the Milky Way dark matter distribution*, [1901.02463](#).

- [106] Y. Wu, K. Freese, C. Kelso and P. Stengel, *Uncertainties in Direct Dark Matter Detection in Light of GAIA*, [1904.04781](#).
- [107] G. L. Kane, P. Kumar, B. D. Nelson and B. Zheng, *Dark matter production mechanisms with a nonthermal cosmological history: A classification*, *Phys. Rev.* **D93** (2016) 063527 [[1502.05406](#)].
- [108] M. Drees, F. Hajkarim and E. R. Schmitz, *The Effects of QCD Equation of State on the Relic Density of WIMP Dark Matter*, *JCAP* **1506** (2015) 025 [[1503.03513](#)].
- [109] M. Kawasaki, K. Kohri and N. Sugiyama, *MeV scale reheating temperature and thermalization of neutrino background*, *Phys. Rev.* **D62** (2000) 023506 [[astro-ph/0002127](#)].
- [110] S. Hannestad, *What is the lowest possible reheating temperature?*, *Phys. Rev.* **D70** (2004) 043506 [[astro-ph/0403291](#)].
- [111] K. Ichikawa, M. Kawasaki and F. Takahashi, *The Oscillation effects on thermalization of the neutrinos in the Universe with low reheating temperature*, *Phys. Rev.* **D72** (2005) 043522 [[astro-ph/0505395](#)].
- [112] F. De Bernardis, L. Pagano and A. Melchiorri, *New constraints on the reheating temperature of the universe after WMAP-5*, *Astropart. Phys.* **30** (2008) 192.
- [113] T. R. Slatyer, *Indirect dark matter signatures in the cosmic dark ages. I. Generalizing the bound on s-wave dark matter annihilation from Planck results*, *Phys. Rev.* **D93** (2016) 023527 [[1506.03811](#)].
- [114] FERMI-LAT collaboration, *The Fermi Galactic Center GeV Excess and Implications for Dark Matter*, *Astrophys. J.* **840** (2017) 43 [[1704.03910](#)].
- [115] DES, FERMI-LAT collaboration, *Searching for Dark Matter Annihilation in Recently Discovered Milky Way Satellites with Fermi-LAT*, *Astrophys. J.* **834** (2017) 110 [[1611.03184](#)].
- [116] F. Pérez and B. E. Granger, *IPython: A System for Interactive Scientific Computing*, *Comput. Sci. Eng.* **9** (2007) 21.
- [117] J. D. Hunter, *Matplotlib: A 2D Graphics Environment*, *Comput. Sci. Eng.* **9** (2007) 90.
- [118] E. Jones, T. Oliphant, P. Peterson et al., *SciPy: Open source scientific tools for Python*, 2001–.